

Static Holes in the Geometrically Frustrated Bow Tie Ladder

George B. Martins

Department of Physics, Oakland University, Rochester, MI 48309, U.S.A.

Wolfram Brenig

Institut für Theoretische Physik, Technische Universität Braunschweig, D-38106 Braunschweig, Germany

(Dated: November 10, 2018)

We investigate the doping of a geometrically frustrated spin ladder with static holes by a complementary approach using exact diagonalization and quantum dimers. Results for thermodynamic properties, the singlet density of states, the hole-binding energy and the spin correlations will be presented. For the undoped systems the ground state is non-degenerate, with translationally invariant nearest-neighbor spin correlations. In the doped case, we find that static holes polarize their vicinity by a localization of singlets in order to reduce the frustration. This polarization induces short range repulsive forces between two holes and an oscillatory behavior of the long range two-hole energy. For most quantities investigated, we find very good agreement between the quantum dimer approach and the results from exact diagonalization.

PACS numbers: 75.10.Jm, 75.30.Hx, 75.40.Mg

I. INTRODUCTION

Geometric frustration is a key factor, leading to exotic phases in quantum spin systems. Valence bond (VB) ordering, with and without breaking of discrete lattice symmetries, is one possible type of ground state symmetry. Examples are the spin-1/2 zig-zag ladder¹, the checkerboard lattice^{2,3}, the j_1 - j_2 - j_3 model^{4,5}, or the Shastry-Sutherland model⁶. Another exotic phase is the spin liquid (SL) which displays no apparent magnetic order but may break topological symmetries, which presumably is the case for the two-dimensional (2D) spin-1/2 kagomé antiferromagnet (AFM)^{7,8,9}.

Static holes, i.e. nonmagnetic defects, are an important probe of such quantum phases. In case of enhanced VB correlations or VB order without broken lattice symmetries, the situation is similar to spin-ladders and the 2D Heisenberg AFM, where static holes generate spin-1/2 moments in their vicinity^{10,11,12}. The latter induce triplet excitations at low-energies. In a SL, e.g. in the kagomé AFM, a very different scenario has been observed, in which singlet pairs accumulate close to the holes, rather than spin-1/2 moments¹³. In case of VB states with spontaneous breaking of the lattice symmetry¹⁴, and other valence-bond ground states,¹⁵ bound spin-1/2 moments also seem to be absent. Apart from the properties of a single static hole, correlation effects between two holes may shed light on the (de)confinement of mobile carriers in frustrated quantum magnets^{16,17,18,19} - at least for kinetic energies small compared to the exchange coupling, i.e., $t \ll J$. Along this line, hole-hole interactions have been studied recently in the kagomé AFM¹³ and in quantum dimer models²⁰. In both cases, deconfinement of the static holes has been found. For two recent μ SR-studies of doped kagomé AFMs, see refs. 21,22.

Additional insight into the response of frustrated spin models to static holes can be obtained from a reduced

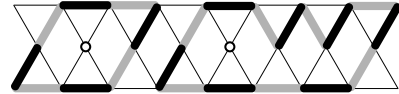


Figure 1: 1D Bow-Tie lattice structure of corner sharing triangles. Spin-1/2 moments reside on all vertices. Thick grey (black) bonds correspond to one QD configuration. Combination of grey and black QDs represent one transition graph. Circles at the center correspond to two static holes.

description of the singlet sector in terms of short-range resonating valence-bonds²³, so-called quantum dimers (QDs)^{9,24}. Classical dimer models on bipartite lattices allow for a height representation and tend to be confining, with a linearly or logarithmically attractive ‘string potential’ between holes^{25,26}. Non-bipartite lattices lack a height representation and allow for both, confining as well as deconfining^{27,28,29,30,31} phases. Similar behavior is likely for QD models.

In this work we intend to shed further light on the role of static holes in geometrically frustrated magnets by studying the spin-1/2 AFM on a bow-tie ladder (BTL). The BTL is a one-dimensional array of corner sharing triangles, as depicted in Fig. 1, and may be viewed as the medial lattice of the two-leg ladder²⁹. The AFM Heisenberg model on the BTL with nearest-neighbor exchange

$$H = \sum_{\langle lm \rangle} \mathbf{S}_l \cdot \mathbf{S}_m \quad (1)$$

has been investigated extensively by linear spin wave theory, exact diagonalization (ED) and density matrix renormalization group (DMRG) in ref. 32. This analysis has uncovered several issues which remain open. In particular, ED on up to $N = 30$ sites suggests that the BTL is qualitatively similar to the Kagomé AFM, i.e. the system is a SL with a spin gap and a large number of singlets ($\propto N^2$) below the first triplet. However, ED does not allow extrapolation of the triplet gap to the thermody-

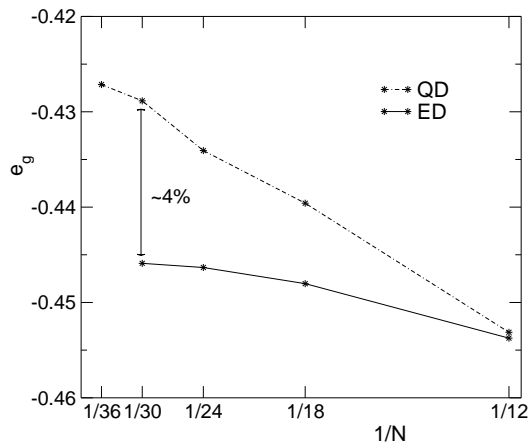


Figure 2: Ground state energy versus inverse system size for $N = 12 - 30$ (ED) and $N = 12 - 36$ (QD).

dynamic limit. DMRG up to $N = 120$ indicates a vanishing spin gap for $N \rightarrow \infty$. Therefore, apart from a SL state it remains possible that the BTL is critical or displays VB order with a very large unit cell.

Here, we will not focus on these properties of the clean BTL in the thermodynamic limit. Instead, we will investigate the local correlations of *two static holes* - holons hereafter - introduced into finite BTLs. To this end, results from two complementary methods will be discussed, namely, complete ED on the one hand, and restricted diagonalization in the QD subspace on the other hand. Recently, QDs on a BTL lattice have been considered, for the so-called μ -model of shortest length resonance-moves for the QDs. There, for certain *ad-hoc* resonance amplitudes the QD model was shown to be identical to the transverse-field Ising chain at criticality²⁹. In contrast to that study, we will account for all resonance moves resulting from eqn. (1).

II. THERMODYNAMIC PROPERTIES

First, we briefly consider the clean system and compare the ground state energy and specific heat, obtained by ED, with results from the QD approximation. The generalized eigenvalue problem in the QD Hilbert space uses the transition graphs depicted in Fig. 1 and is set up according to ref. 33 (to which we refer the reader for details). Periodic boundary conditions (PBC) apply to all results discussed in the following. For all systems studied we find the undoped ground state to be non-degenerate, with translationally invariant nearest-neighbor spin correlations, which is consistent with a spin liquid state or a valence bond crystal with a unit cell large compared to the system's sizes. In Fig. 2, we show the ground state energy e_g versus the inverse system size $1/N$. For QDs, proper N needs to be a multiple of 6. From Fig. 2, a deviation of approximately 4-5% between ED and QD can be extrapolated in the thermodynamic limit. This has to be contrasted against the relative dimension D

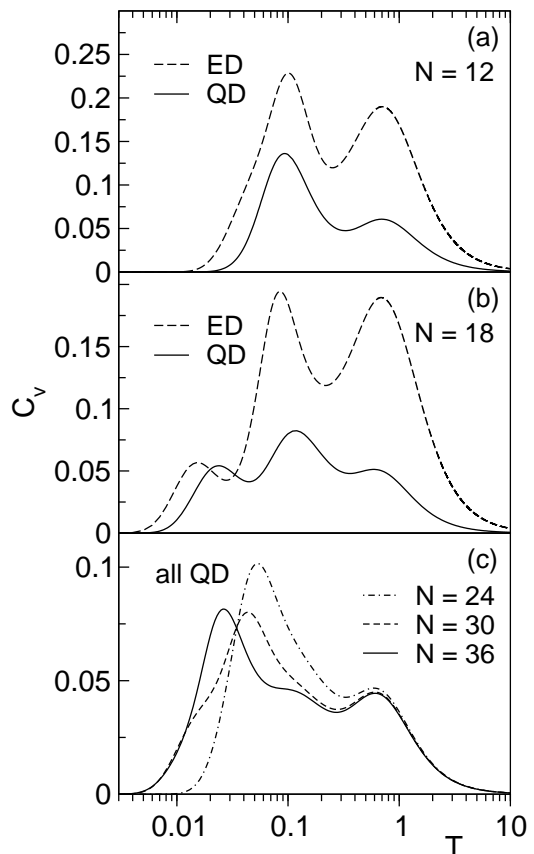


Figure 3: Specific heat C_V versus temperature T . (a) and (b): comparison of ED and QD for $N = 12$ and 18. (c) QD for $N = 24-36$.

of the complete Hilbert space, D_0 of the singlet sector, and D_{QD} of the QD space, which are $D = 2^N$, $D_0 = N! / [(N/2)!(1 + N/2)!]$, and $D_{QD} = 2^{N/3+1}$. For $N=30$, this implies $D/D_0/D_{QD} \approx 1.1 \cdot 10^9 / (9.7 \cdot 10^6) / (2.0 \cdot 10^3)$. In view of these ratios, the results in Fig. 2 are in reasonable agreement. The figure shows a very small ‘even/odd’ oscillation with respect to $N/6$ in the QD results.

A fingerprint of SL states in strongly frustrated magnets is the accumulation of singlet states at low energies. In the kagomé AFM, the number of singlets below the first triplet has been observed to grow exponentially with system size⁸. In the BTL, power-law behavior with an exponent 2 has been suggested³². The singlet accumulation at low-energies leads to a characteristic singlet-triplet double-peak structure in the specific heat C_V ^{7,32,34,35}. For the kagomé AFM a substantial fraction of the singlet-peak in C_V is believed to be due to QD fluctuations³³. For the BTL, this is an open issue. Therefore, in Fig. 3 we consider C_V from QD and ED calculations. The latter agree with identical results from ref. 32. In view of large finite-size effects our emphasis is on a comparison at identical system sizes, rather than in the thermodynamic limit. First, there is a remarkable similarity between the positions of peaks in ED and QD in Fig. 3(a,b). Second, for the leftmost peak in Fig. 3(b), at low temperatures, the magnitude of C_V and the entropy from ED and QD

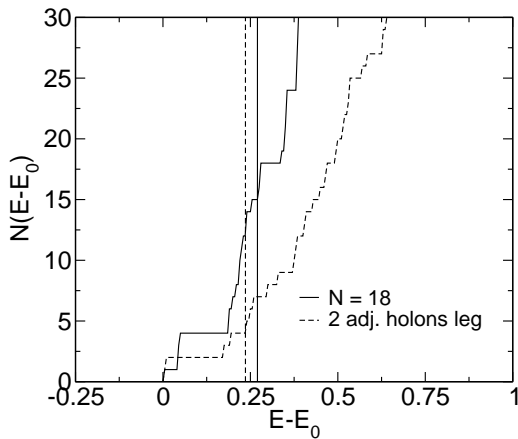


Figure 4: Number of singlets in ED versus energy at $N = 18$, contrasting 0 holons (solid line) with 2 holons (dashed). Solid (dashed) vertical line: triplet gap for 0 (2) holons. Holons are located at two adjacent sites on one BTL leg. E_0 refers to ground state energy.

are comparable. I.e., we conclude that the low- T peak in C_V of the BTL is caused primarily by QD fluctuations. As can be seen from Fig. 3(c), the low- T peak stabilizes as N increases. Third, in the high-energy region $T \gtrsim 0.5$ a single peak can be observed which contains most of the entropy (note the log T -scale). This entropy is significantly larger in the ED as compared to the QD. This difference is due to triplet excitations not present in the QD space. Fig. 3(c) shows that C_V from QD has converged to the thermodynamic limit for $T \gtrsim 0.1$ at $N > 36$ - a system size we cannot reach with ED. Finally, the intermediate- T feature in ED seems strongly system-size dependent, as already noted in ref. 32.

III. STATIC HOLES

In this section, we consider the change in the singlet density-of-states (DOS), the binding energy, and the spin correlations which stem from introducing two holons into the BTL.

A. Density of States

Fig. 4 shows the integrated singlet DOS versus energy, contrasting the case of zero holons against that of two holons placed at adjacent sites on the leg of a BTL with an even number of sites. The main point of this figure is the number of singlets below the first triplet. Evidently this number is reduced by introducing the holons. A similar effect is observed for any other relative separation of the holons and also in the case of a single holon. This low-energy suppression of singlet DOS originates from the reduction of frustration at the neighboring sites of the holons, which favors binding of singlets in the vicinity of the holons (see also section III C). Consequently the

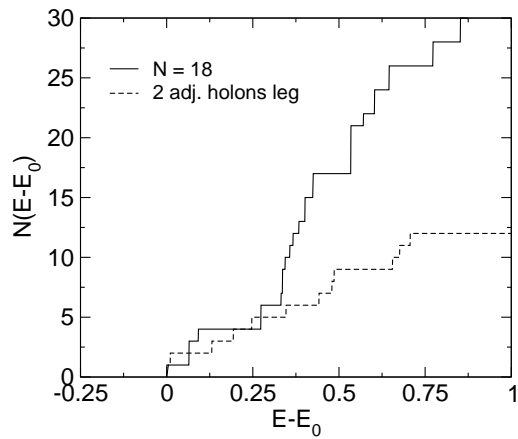


Figure 5: Number of QD singlets versus energy at $N = 18$, contrasting 0 holons (solid line) with 2 holons (dashed). Holons are located at sites identical to Fig. 4. E_0 refers to ground state energy.

low-energy singlet DOS decreases, while the triplet gap is set by excitations distant from the holons and therefore less affected. While similar effects have been reported for the kagomé AFM¹³, this behavior is drastically different from VB states on bipartite lattices, where static holes tend to bind spin-1/2 moments which leads to an increase of low-energy triplet DOS³⁶.

While the QD variational space does not contain triplet excitations, it is nevertheless instructive to compare the impact of holons on the singlet DOS between the ED and QD calculations. In Fig. 5, we show the number of singlets above the ground state energy in the QD case for a system size and a holon placement identical to that of Fig. 4. First, the overall trend for QDs depicted is remarkably similar to that in ED. Second, the suppression sets in at somewhat larger energies, of $E-E_0 \sim 0.3$ for QDs, as compared to $E-E_0 \sim 0.2$ for ED. Finally, it can be seen that in the energy window depicted the QD singlets make up for approximately 50% of the total number of singlets in ED.

B. Two-holon Energy

Now, we turn to the binding energies

$$\Delta e_{2h}^a(L) = E_0^a(L) - E_0^a(L=1) \quad (2)$$

of two holons separated by L sites along the center(leg) = a of the BTL, where E_0^a refers to the corresponding ground state energies. In Figs. 6 and 7 we present two aspects of $\Delta e_{2h}^a(L)$. In the former, we compare the binding energies obtained from ED with those from QDs for various systems sizes. First, and remarkably, the ED and QD results are very similar, both for $a = \text{center}$ and leg . Second, these figures demonstrate that the holons experience a short range repulsive force, with a maximum binding energy at approximately 3 lattice sites. This is in sharp contrast to quantum AFMs with VB ground

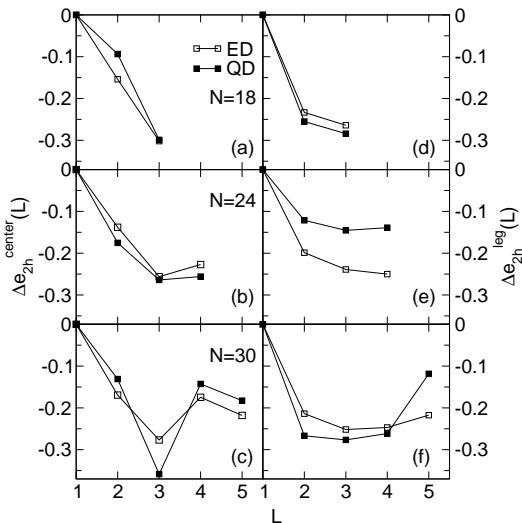


Figure 6: Comparing two-holon energies at holon separation L from ED (solid line with open squares) with QDs (solid line with solid squares) for different systems sizes $N=18, 24$, and 30 . (a)-(c) [(d)-(f)] refer to two holons in [on] the center [leg] of the BTL.

states on bipartite lattices. There, two holons experience a maximum binding energy if placed on those nearest-neighbor sites which are occupied by singlet dimers in the undoped case. Moreover, separating the holons will generate a string of ‘misplaced’ dimers of length proportional to the holon separation. This generates a confining potential. Such confinement cannot be inferred from Fig. 6. Rather, from the largest system which allows for a direct comparison between ED and QDs, i.e. $N=30$, an oscillatory behavior at large distances can be anticipated. This can be corroborated by extending the QD calculation to larger system sizes as shown in Fig. 7. There, clear oscillations in $\Delta e_{2h}^a(L)$ can be observed in the right panel, both on the legs and in the center. In the next section, an intuitive picture of the two-holon energies in terms of the dimer coverings will arise. From the preceding, it is tempting to speculate that mobile holons on the BTL are bound only weakly and will deconfined already for kinetic energies small compared to J .

Finally, Fig. 7 points towards some of the limitations of the QD approach. While the qualitative behavior is identical for ED and QDs, i.e. panels (a) vs. (c) and (b) vs. (d), panel (d) shows a significant variation of the absolute value of the QD binding energies, depending on whether $N/6$ is even or odd. The latter even/odd effect is absent in the ED results.

C. Spin-Spin Correlations

The nearest-neighbor spin-spin correlations $s_{lm} = \langle \mathbf{S}_l \cdot \mathbf{S}_m \rangle$ are a direct measure of the singlet amplitude on the bond lm . Here, we consider the impact of two holons on s_{lm} at zero temperature. Fig. 8 summarizes

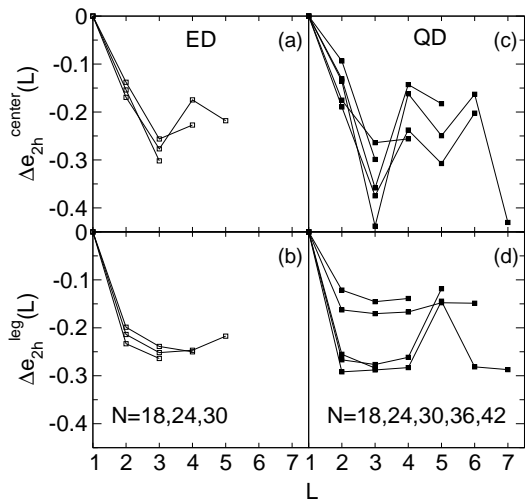


Figure 7: Evolution of two-holon energies at holon separation L with system size for ED (solid line with open squares) with $N=18-30$ in (a), (b) and for QDs (solid line with solid squares) with $N=18-42$ in (c), (d).

our results, both for ED and QDs on the largest system for which we have performed ED, i.e. $N=30$. In this figure s_{lm} is visualized in terms of ‘bond-thickness’. First, we note that s_{lm} fulfills the sum rule

$$E_0(L) = \sum_{lm} s_{lm} \quad (3)$$

where $E_0(L)$ refers to the ground state energy with two holons in a relative configuration denoted by L . Using the results from Figs. 6, 7, and 2, the sum rule has been checked to hold for all cases we have studied, both for ED and QDs and also for the undoped case, which will not be discussed here. From Fig. 8, it is evident that the holons introduce a strong polarization into the magnetic background, which leads to spatial oscillations of the spin-spin correlations, with a pattern depending on the separation of the holons. This has to be contrasted against the undoped case, in which s_{lm} is almost homogeneous along the BTL with only a very small transverse difference between the central rungs and the legs. Specifically, the figure demonstrates that s_{lm} tends to be largest in the vicinity of the holons. This corroborates the picture of a doping induced reduction of singlet fluctuations, due to singlet-binding to the holons as discussed in Sec. III A. In fact, the maximal values of $|s_{lm}|$ in the vicinity of the holons as shown in the figure are close to $3/4$, implying a singlet amplitude of 1 on those bonds. Note that for a small number of bonds, ferromagnetic correlations of a rather small absolute magnitude arise, both in ED and for QDs.

The tendency of the system to accommodate singlets next to the holons provides for a direct interpretation of the holon-repulsion, namely the number of ‘strong’ singlets which can be bound to the vicinity of the holons is less if their separation is small. This can be read off directly from Fig. 8 in going from panel 1) to 5).

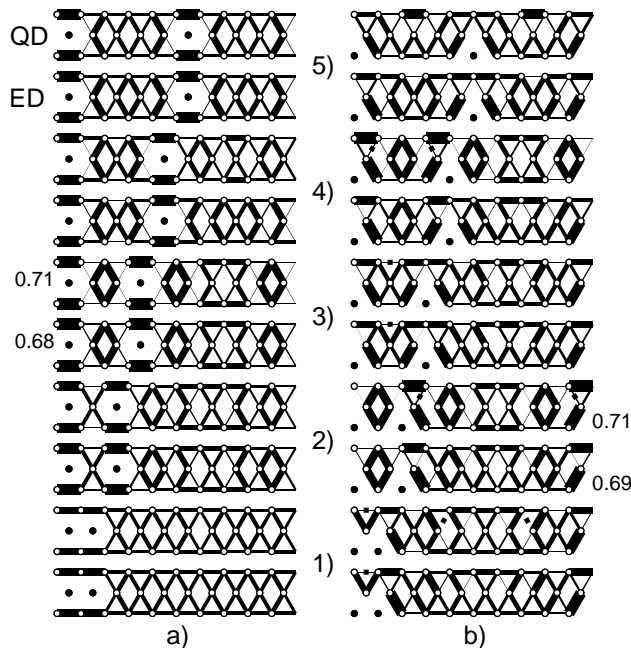


Figure 8: Nearest neighbor spin-spin correlations s_{lm} from ED and QDs, for two holons (full circles) on the center and leg of a BTL with $N = 30$ for a) and b). The width of solid lines (with vertical slash) is a linear measure of $-s_{lm}$ ($s_{lm} < 0$ (> 0)). 1)...5) labels all non-equivalent two-holon positions. For each 1)...5) the adjacent lower (upper) graph corresponds to one ED (QD) result, both for a) and b). Numbers refer to maximum values of $-s_{lm}$ observed for ED and QDs in a) and b).

For the majority of holon placements depicted in Figs. 8a) and b), namely a) 1), 2), 3), and 5) as well as b) 1), 2), and 3), the qualitative real-space structure of s_{lm} is remarkably similar for ED and QDs. For group a) 4) there are some differences observable right of the second holon. In groups b) 4) and 5) there are clear qualitative differences between ED and QDs, especially on the leg free of holons. This suggests that QDs provide for a better description of holons in the ‘bulk’ of the BTL than on its boundaries.

For a quantitative comparison between ED and QDs, we turn to Fig. 9, where we show several cuts along the BTL through the legs and rungs displaying the values of $-s_{lm}$ versus a measure of distance given by a ‘1D center-of-mass’ CM of each bond. CM runs in steps of 2 ($1/2$) from 0 ($-1/2$) to $2N/3 - 2$ ($2N/3 - 3/2$) on the legs (rungs). The top four panels in Fig. 9 are representative of those cases in Fig. 8 which suggest qualitative agreement between ED and QD. It is readily apparent that there is also excellent quantitative agreement. The lower two panels in Fig. 9 refer to $-s_{lm}$ on the upper leg (rung) for the worst case of Fig. 8 b) 5), where ED and QD show strong qualitative differences.

In the following, we provide additional discussion of the results shown in Figs. 6 - 9. When both holons are positioned in the center axis (see Fig. 8a), reflection symmetry around this axis is retained. This allows

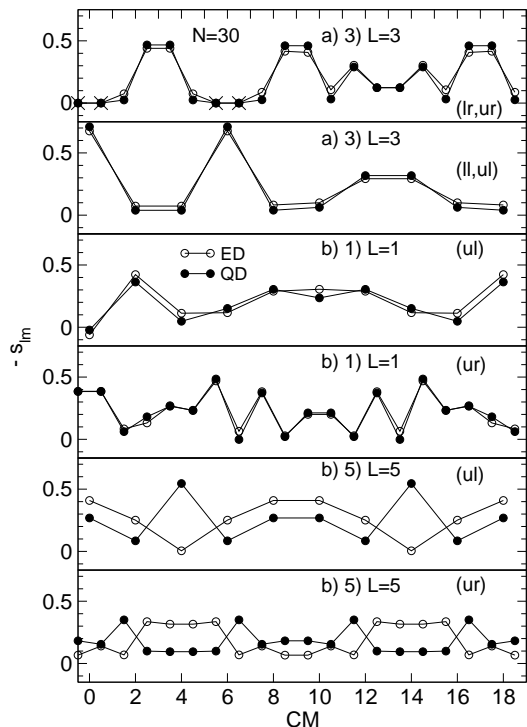


Figure 9: Negative nearest neighbor spin-spin correlations $-s_{lm}$ along the upper(lower) leg(rung) for u(l)|l(r) from ED(QDs) for open(closed) circles with two holons and $N=30$, corresponding to Fig. 8 and panels a) 3), b) 1), and b) 5). CM labels ‘center of mass’ of bonds. Crosses mark bonds linked to holons where s_{lm} has been set to 0.

for the formation of highly symmetric and simple spin structures. First, as noted above, isolated singlets form at the bonds situated closest to the holons for all holon separations. Second, more subtle geometrical constraints decide if other spin structures (e.g., loops with even numbers of spins or short chains) will form, where they will be located, and how much singlet correlations there will be between them. For example, in Fig. 8a) 3), at a holon distance of $L = 3$, apart from the four isolated dimers, one can clearly notice the presence of 4- and 8-spin loops in the shape of three diamonds and a four-pointed star, respectively. These structures are only weakly connected by singlet correlations³⁷. Obviously, the distance between the holons is one of the controlling parameters in this respect. For example, at distance $L = 5$, open 3-spin chains are present in the shape of boomerangs, besides diamonds and dimers. However, in this case, these structures are not as independent from each other, i.e., the singlet links between them are stronger, as compared to $L = 3$. Therefore, some holon distances are more favorable than others in allowing for the formation of such independent ‘frustration releasing’ structures. This leads to the oscillating behavior of the binding energy in Fig. 7c)³⁸. Finally, since weakly connected dimers, boomerangs, and diamonds can be described rather well by the QD basis, the very good quantitative agreement between ED and QD for holons located in the center axis

is no surprise.

When the holons are both on the same leg, reflection symmetry around the central axis is lost. Therefore, apart from the dimers close to the holons, simple structures as described above are less favorable and form only for some holon distances, as for example the diamonds seen at $L = 2$ in Fig. 8b). Instead, and in contrast to the centered holons, more complex correlations of the spins occur, which involve the presence of ‘spin chains’ of considerable length. These cannot form when the holons are in the center axis because of symmetry considerations and avoidance of uncorrelated free spins. These chain structures with longer range spin-spin correlations are not well described by the QD basis. Their presence leads to quantitative discrepancies with the ED results. The difference in agreement between Fig. 7(a) and (c) versus Fig. 7(b) and (d), as well as the discrepancies in the two lower two panels in Fig. 9 corroborate this interpretation³⁹.

IV. CONCLUSIONS

In summary, we have performed a complementary numerical analysis of a geometrically frustrated quantum spin ladder with and without static holes using exact diagonalization and a truncated basis of quantum dimers.

For the undoped system, we have shown that dimers allow for a reasonable approximation of the ground state energy and the low temperature specific heat. In the doped case, we have shown that the system can release frustration through binding of singlets and other extended unfrustrated spin structures to the static holes. Results for the holon binding energies and the nearest-neighbor spin correlations confirm this picture. Analysis of dynamic correlation functions, as e.g. magnetic Raman scattering, and the finite size scaling of overlaps between ED and QD states, will be presented elsewhere⁴⁰.

Acknowledgments

Fruitful discussions with E. Dagotto and A. Albuquerque are gratefully acknowledged. One of us (W.B.) acknowledges the kind hospitality of the National High Magnetic Field Laboratory at Florida State University in the early stages of this project. Part of this work has been supported by DFG grant No. BR 1084/2-2 and BR 1084/2-3. G.M. acknowledges support from Research Corporation (Contract No. CC6542). G.M. thanks E. Dagotto for the use of a 32 Gigabytes Altus 3400 quad-Opteron workstation located at University of Tennessee in Knoxville.

-
- ¹ C. K. Majumdar and D. K. Ghosh, *J. Math. Phys.* **10**, 1388 (1969); *ibid.*: **10**, 1399 (1969)
 - ² W. Brenig and A. Honecker, *Phys. Rev. B* **65**, 140407 (2002).
 - ³ J. B. Fouet, M. Mambrini, P. Sindzingre, and C. Lhuillier, *Phys. Rev. B* **67**, 054411 (2003).
 - ⁴ R. R. P. Singh, Z. Weihong, C. J. Hamer, and J. Oitmaa, *Phys. Rev. B* **60**, 7278 (1999).
 - ⁵ M. Mambrini, A. Läuchli, D. Poilblanc, F. Mila, *Phys. Rev. B* **74**, 144422 (2006).
 - ⁶ B. S. Shastry and B. Sutherland, *Physica B & C* **108**, 1069 (1981).
 - ⁷ C. Zeng and V. Elser, *Phys. Rev. B* **42**, 8436 (1990).
 - ⁸ C. Waldtmann, H.-U. Everts, B. Bernu, C. Lhuillier, P. Sindzingre, P. Lecheminant, and L. Pierre, *EPJ B: Condensed Matter and Complex Systems* **2**, 501 (1998).
 - ⁹ G. Misguich and C. Lhuillier, in ‘Frustrated spin systems’, H. T. Diep editor, World-Scientific. ISBN 981-256-091-2 (2005).
 - ¹⁰ G. B. Martins, E. Dagotto, and J. A. Riera, *Phys. Rev. B* **54**, 16032 (1996).
 - ¹¹ M. Laukamp, G. B. Martins, C. Gazza, A. L. Malvezzi, E. Dagotto, P. M. Hansen, A. C. López, and J. Riera, *Phys. Rev. B* **57**, 10755 (1998).
 - ¹² S. Wessel, B. Normand, M. Sgrist, and S. Haas, *Phys. Rev. Lett.* **86**, 1086 (2001).
 - ¹³ S. Dommange, M. Mambrini, B. Normand, and F. Mila, *Phys. Rev. B* **68**, 224416 (2003).
 - ¹⁴ B. Normand and F. Mila, *Phys. Rev. B* **65**, 104411 (2002).
 - ¹⁵ A. K. Kolezhuk, *J. Phys.: Condens. Matter* **10**, 6795 (1998).
 - ¹⁶ N. Read and S. Sachdev, *Phys. Rev. Lett.* **66**, 1773 (1991).
 - ¹⁷ T. Senthil, A. Vishwanath, L. Balents, S. Sachdev, and M. P. A. Fisher, *Science* **303**, 1490 (2004).
 - ¹⁸ F. Pollmann and P. Fulde, *Europhys. Lett.* **76**, 133 (2006).
 - ¹⁹ D. Poilblanc, A. Läuchli, M. Mambrini, and F. Mila, *Phys. Rev. B* **73**, R100403 (2006).
 - ²⁰ G. Misguich, D. Serban, and V. Pasquier, *J. Phys.: Condens. Matter* **16**, S823 (2004).
 - ²¹ A. Fukaya, Y. Fudamoto, I. M. Gat, T. Ito, M. I. Larkin, A. T. Savici, Y. J. Uemura, P. P. Kyriakou, G. M. Luke, M. T. Rovers, K. M. Kojima, A. Keren, M. Hanawa, and Z. Hiroi, *Phys. Rev. Lett.* **91**, 207603 (2003).
 - ²² D. Bono, P. Mendels, G. Collin, N. Blanchard, F. Bert, A. Amato, C. Baines, and A. D. Hillier, *Phys. Rev. Lett.* **93**, 187201 (2004).
 - ²³ P. Anderson, *Science* **235**, 1196 (1987).
 - ²⁴ D. Rokhsar and S. Kivelson, *Phys. Rev. Lett.* **61**, 2376 (1988).
 - ²⁵ M. E. Fisher and J. Stephenson, *Phys. Rev. B* **132**, 1411 (1963).
 - ²⁶ F. Wu, cond-mat/0303251, unpublished.
 - ²⁷ G. Misguich, D. Serban, and V. Pasquier, *Phys. Rev. Lett.* **89**, 137202 (2002).
 - ²⁸ P. Fendley, R. Moessner, and S. L. Sondhi, *Phys. Rev. B* **66**, 214513 (2002).
 - ²⁹ G. Misguich, D. Serban, and V. Pasquier, *Phys. Rev. B* **67**, 214413 (2003).
 - ³⁰ W. Krauth and R. Moessner, *Phys. Rev. B* **67**, 064503 (2003).

- ³¹ A. D. Huse, W. Krauth, R. Moessner, and S. L. Sondhi, Phys. Rev. Lett. **91**, 167004 (2003).
- ³² C. Waldtmann, H. Kreutzmann, U. Schollwöck, K. Maisinger, and H.-U. Everts, Phys. Rev. B **62**, 9472 (2000).
- ³³ C. Zeng and V. Elser, Phys. Rev. B **51**, 8318 (1995).
- ³⁴ V. Elser, Phys. Rev. Lett. **62**, 2405 (1989).
- ³⁵ A. P. Ramirez, B. Hessen, and M. Winklemann, Phys. Rev. Lett. **84**, 2957 (2000).
- ³⁶ W. Brenig, preprint cond-mat/0606269 (2006).
- ³⁷ The analysis of figures similar to Fig. 8 for smaller clusters (not shown) presents the same picture, i.e., at distance $L = 3$ (holons in center axis) these simple structures are very well defined and quite weakly connected to each other, resulting in a strong binding energy for holons at this particular distance.
- ³⁸ It is interesting to note that a criterion that appears to be followed in the formation of these structures is the avoidance of isolated 'free' spins.
- ³⁹ The presence of these spin-chain structures is easier to spot in spin-spin correlations for smaller clusters than the one shown in Fig. 8 (with 30 sites). Therefore, the study of varying cluster sizes at constant holon doping is needed for a more detailed analysis of the properties of these structures.
- ⁴⁰ G. Martins and W. Brenig, in preparation.